A new high-pressure technique for the measurement of low frequency seismic attenuation using cyclic torsional loading

Jean-Philippe Perrillat, Roman Bonjan, Yann Le Godec, Frédéric Bergame, Julien Philippe, Mohamed Mezouar, Gaston Garbarino, Andrew King, Nicolas Guignot

A new high-pressure technique for the measurement of low frequency seismic attenuation using cyclic torsional loading

J.P. Perrillat[1,(a)], R. Bonjan[1], Y. Le Godec[2], F. Bergame[2], J. Philippe[2], M. Mezouar[3], G. Garbarino[3], A. King[4], N. Guignot[4]

[1] Université de Lyon, Université Lyon 1, Ens de Lyon, CNRS, UMR 5276 Lab. de Géologie de Lyon, 69622 Villeurbanne, France
[2] Sorbonne Universités, CNRS, UMR 7590 Institut de Minéralogie de Physique des Matériaux et de Cosmochimie, 75252 Paris, France
[3] European Synchrotron Radiation Facility, 38043 Grenoble, France
[4]Synchrotron SOLEIL, BP 38, Saint‑Aubin, 91192 Gif‑sur‑Yvette, France

[(a)] Author to whom correspondence should be addressed: jean-philippe.perrillat@univ-lyon1.fr

ABTRACT

We report a new technique for torsional testing of materials under giga-pascal pressures, which uses a shearing module in a large volume Paris-Edinburgh press in combination with high-resolution fast radiographic X-ray imaging. The measurement of the relative amplitude and phase lag between the cyclic displacement in the sample and a standard material (Al_2O_3) provides the effective shear modulus and attenuation factor for the sample. The system can operate in the 0.001 to 0.01 Hz frequency range, and up to 5 GPa and 2000 K; although high-temperature measurements may be affected by grain growth and plastic strain. Preliminary experimental results on San Carlos olivine are in quantitative agreement with previously reported Q^{-1} factors at lower pressure. This cyclic torsional loading method opens new directions to quantify the viscoelastic properties of minerals/rocks at seismic frequencies and in pressure-temperature conditions relevant to the Earth's mantle, for a better interpretation of seismological data.

INTRODUCTION

The Earth's materials are viscoelastic solids characterized by a continuous change from elastic behavior at high frequencies and/or low temperatures to viscous behavior at low frequencies and/or high temperatures (*e.g.* Jackson, 2008). This anelastic behavior of rocks is evidenced by seismic attenuation that manifests through the decrease in amplitude and energy of seismic waves as they propagate inside the Earth (*e.g.* Aki and Richards, 1980). This viscoeleastic relaxation is responsible for dispersion, *i.e*. the frequency dependence, of seismic wave velocities. It is generally quantified in seismology by the quality factor *Q* (or its reciprocal

loss factor Q^{-1}) defined as $Q = 2\pi E/\Delta E$, where E is the energy of seismic wave and ΔE is the energy change per cycle (Knopoff, 1964). The relaxation processes in rocks are controlled by the temperature, composition, grain size, melt/volatile content, and a number of other physical and chemical factors of the rocks (*e.g.* Karato and Spetzler, 1990; Cooper, 2002; Jackson, 2008). For this reason, seismic attenuation is a potential rich source of information about the Earth's interior, complementary to seismic velocities. Over the last decade, seismologists have made striking progress in mapping seismic attenuation, parametrized in terms of the quality factor Q, either at the regional (Stachnik *et al*., 2004; Pozgay *et al*., 2009) or global scale (Gung and Romanowicz, 2004; Adenis *et al*., 2017). However, attempts to translate Q values into meaningful quantitative physico-chemical parameters have been hampered by the lack of experimental data on the anelasticity of rocks at the relevant high pressure-temperature (P-T) conditions and low frequencies of teleseismic waves (mHz-Hz).

Laboratory measurements of attenuation Q^{-1} involves cyclic-loading methods that measure the dynamic mechanical response of a material to an applied stress (*e.g.* Guéguen and Palciauskas, 1994). These involve either axial or torsional forced-oscillation tests, where the sample and an elastic standard of known modulus and negligible dissipation are connected in series and subjected to a low-frequency sinusoidal time varying stress. For the elastic standard the resulting strain is in phase with the applied stress with an amplitude inversely proportional to its elastic modulus. Similarly, for the investigated sample, except that its viscoelastic behaviour is manifest in a phase lag ($\Delta\delta$) of strain behind stress. Thus the measurement of the relative amplitudes and phases of the cyclic displacements in standard and sample provides the elastic modulus, and the strain energy dissipation ($Q^{-1} = \tan(\Delta\delta)$) respectively, for the sample. The measurements must be performed in the linear domain (*i.e.* where the stress response is linearly proportional to strain) so that the elastic modulus and internal friction Q^{-1} are independent of strain amplitude. The upper limit of strain in the linear region depends on materials, for example, 10^{-2} for alumina (Ota and Pezzotti, 1996). Therefore, for mm-size sample, the displacement strain to be observed is usually of the order of few microns.

Torsion pendulum devices have been successfully applied at high-temperature and room pressure to explore the anelastic properties of minerals (Guéguen *et al.,* 1981, Gribb and Copper, 1998), and solid or partially molten rocks (Berckhemer *et al.* 1982, Bagdassarov and Dingwell, 1993). However, these early measurements suffered from the creation of porosity through thermal microcracking and the complex behavior of interfaces within the experimental assembly. To overcome these limitations, Jackson and Paterson (1993) implemented the forced-oscillation technique in an internally heated gas-charged pressure vessel. In this device, a pair of electromagnetic drivers housed within the pressure vessel provides for the generation of the

torque, and the twist of the assembly is measured above and below the elastic standard by pairs of parallel plate capacitance transducers. The frequency-dependence of the shear modulus and dissipation has been determined in this device in a variety of polycrystalline materials like olivine (Jackson *et al*., 2002), MgO (Webb and Jackson, 2003) or titanate perovskites (Webb *et al.*, 1999). However, the maximum accessible pressure within this device is 0.3 GPa, which is a major limitation to the application of attenuation data to the Earth's mantle.

The effect of pressure on a general anelastic response is manifested by an activation volume that might be significant at giga-pascal pressures. Furthermore, pressure commonly induces structural changes in minerals which act to modify mechanical properties, both elastic and anelastic. Such properties clearly need to be understood at the high P-T conditions of stability of the phases involved. The challenge in applying the cyclic loading method in the giga-pascal pressure domain is the need of a technique for measuring stress and strain with sufficient precision, and with sufficiently short measurement time, while the sample is embedded in a high-pressure vessel. Recently, several studies demonstrated these difficulties can be overcome by the use of synchrotron radiography. Li and Weidner (2008) and Yoshino *et al*. (2016) reported axial-forced oscillation measurements of Q^{-1} for San Carlos olivine specimen up to 5 GPa and 2000 K in the D-DIA, a large-volume press with capabilities of advancing / withdrawing the top and bottom rams. Change of strain and elastic properties with time is directly observed by X-ray radiography at a specific oscillation frequency. Use of synchrotron X-ray gives an opportunity to determine not only strain but also confining pressure and phase identification. A limitation of this axial-loading method is that it provides the Young's modulus (E). The shear modulus (G) must be converted from the measured Young's modulus using a value for the bulk modulus (K) or the Poisson's ratio (ν) either assumed or from literature data, and the following equations: $G = 3.K.E / (9K-E)$ or $G = E / 2.(1+\nu)$, respectively.

As an alternative, we developed a new high-pressure technique to directly measure the shear modulus (G) dispersion and shear attenuation (Q_G^{-1}) by cyclic torsional loadings (Jackson, 1993). In this paper, we fully describe the experimental set-up that combines a Paris-Edinburgh press with rotating anvils capabilities and synchrotron X-rays. We detail the technical and analytical protocol to determine the anelastic properties from the X-ray monitoring of the sample/standard strain, and discuss the attenuation factor resolution this method can resolve at high P-T and low frequencies. To demonstrate the potential of this new technique, we present a pilot study on strain energy dissipation in polycrystalline San Carlos olivine.

EXPERIMENTAL METHODS

The forced-oscillation high P-T device

To perform the forced-oscillation mechanical testing under high P-T conditions we modified a Paris-Edinburgh cell, a large-volume press based on opposed anvil geometry (Besson *et al*., 1992), to allow for the controlled rotation of the top or bottom anvil under load. Using an X-ray transparent gasket, this geometry offers a large window in the equatorial plane for the *in situ* radiography and diffraction measurements. A detailed mechanical description of this so-called RoToPEc device (for Rotational and Tomography Paris–Edinburgh cell) has been given by Philippe *et al*. (2016). A schematic drawing is shown in **Figure 1**. In brief, the two opposed anvils can rotate independently under load, with no limitation in the rotation angle, through two sets of gear reducers and thrust bearings located at the end of each anvil. The accurate rotation of the anvils is monitored by stepper motors and encoders, with an angular resolution of 0.02°. After pressurization, a sinusoidal stress and strain can be produced on the assembly by rotating the top anvil while the bottom one is held fixed. A Labview software allows to configure the desire sine wave profile by defining the rotation amplitude (in degrees), period (in seconds) and number of cycles. A frequency range from 0.001 to 0.01 Hz and a rotation amplitude from 1 to 5 degrees have been tested so far, and produced resolvable strain on the sample. This cyclic torsional loading system can operate up to 5 GPa and 2000 K for millimeter-size sample (using 10 mm boron-epoxy gasket with tungsten carbide anvils), the main limitation to operate at higher pressure being the reduction of the X-ray window due to the gasket flow under high P-T.

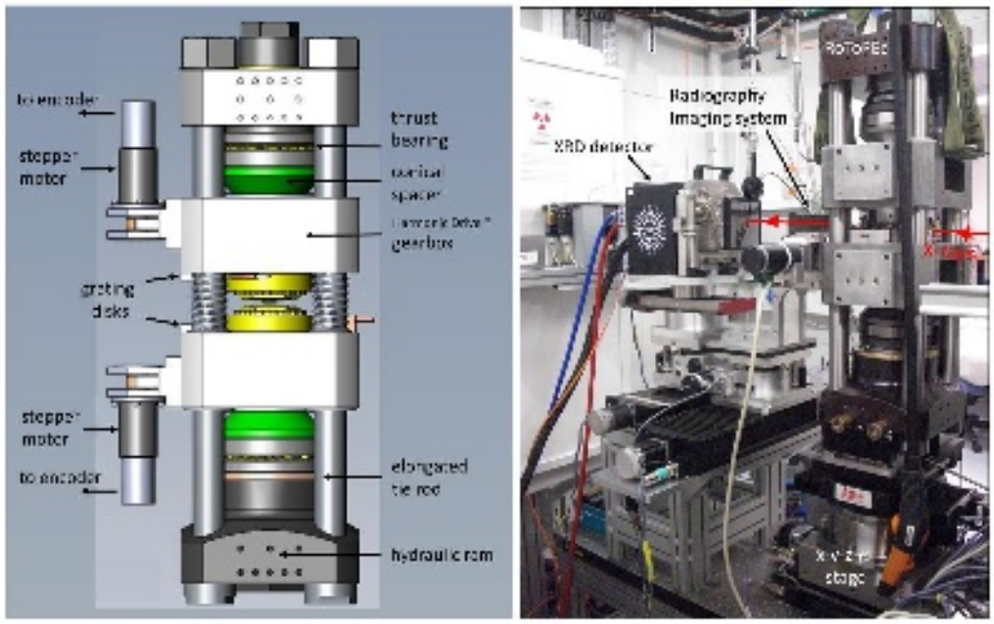

Figure 1 – 3D view of the 450 ton V7 Paris-Edinburgh press with the RoToPEc module, and picture of its installation on beamline ID27 of the ESRF.

Cell assembly

The configuration of the cell assembly used for the forced-oscillation measurements is shown in **Figure 2**. It consists of a biconical boron epoxy gasket of outer diameter of 10 mm and a cylindrical graphite furnace, both transparent to high-energy X-rays. To ensure a transmission of the torque and avoid slippage at interfaces, the sample and elastic standard are directly stacked in between two MgO rods. The sintered polycrystalline specimen and the elastic reference, a dense Al_2O_3 rod (Alfa Aesar^{TM} Al23), are 0.5-0.8 mm in length and 2.9 mm in diameter, both prepared with flat faces polished to mirror quality to be perfectly parallel. The length of MgO rods is adjusted to place the sample and reference material in the center of the X-ray window. A tungsten rod (∅=90 μm) is positioned vertically along the outer diameter of the sample/Al_2O_3 for measuring the twist angle by X-ray absorption. The tungsten rod is actually inserted in a thin groove, made with a diamond file, along the sample/Al_2O_3 cylinder, to ensure a good mechanical coupling between the rod, the sample and the elastic standard. Gold wires (∅=25 μm) are also placed on the top and bottom sides of the sample and alumina reference to measure their lengths during the cycling torsional loadings. The pressure on the sample is derived from the MgO unit-cell volume measured using X-ray diffraction along with the thermoelastic data of Speziale *et al*. (2001). Temperature is estimated by a power-temperature relation curve determined in a previous experiment using a thermocouple and identical cell configuration.

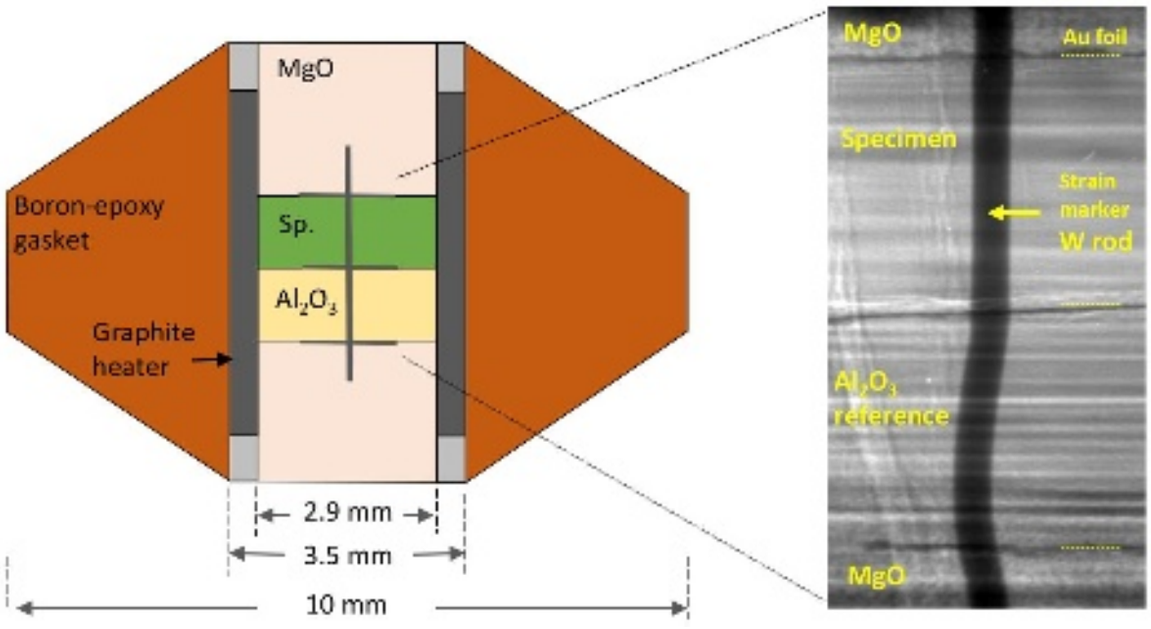

Figure 2 – (left) Cell assembly used for the forced-oscillation measurements, and (right) representative X-ray radiograph through the sample and alumina standard. Highly absorbing features are the gold and tungsten strain markers.

In situ strain measurements

The force-oscillation technique relies on the time-resolved measurement of the twist angles of the sample and elastic reference in response to the sinusoidal imposed torque. The attenuation factor (Q_G^{-1}) of the sample is determined from the phase lag of strain relative to the standard, while the strain amplitude ratio provides a comparative determination of the effective shear modulus (G). A difficulty of the technique is that, in order to be independent of strain amplitude (*i.e.* in the linear viscoelastic domain), extremely small strain variations as 10^{-3} to 10^{-6} depending on the investigated material need to be detected. The use of synchrotron X-ray radiography gives the opportunity to monitor such small displacements, with high precision (micron to sub-micron) and at short periods, by following the motions of strain markers.

In practice, a large X-ray beam illuminates the cell assembly through the transparent gasket. The absorption contrast between the assembly parts, sample, Al_2O_3 reference, and strain markers is converted into visible light by a phosphorous YAG single-crystal set in the transmitted beam on the downstream side of the press. A 45° mirror reflects the visible contrast into a high-speed CCD camera, and the image is focused by an objective lens (**Figure 1**). In this study, measurements have been obtained during two sessions performed at beamline ID27 of ESRF (Mezouar *et al*., 2005) and beamline PSICHE of Synchrotron SOLEIL (King *et al*., 2016). At ID27, the monochromatic 33 keV beam has a field of view of 2.0 and 2.7 mm in the vertical and horizontal directions, respectively. The CCD camera is a CoolSNAP HQ2 (Photometrics) which allows the acquisition of 745 x 413 pixel images at time intervals down to 100 ms. The magnification of the imaging system leads to a pixel size of 2.2 μm. At PSICHE, a pink beam with an average energy of 45 keV is collimated to 2.5 mm and 4.5 mm in the vertical and horizontal directions, respectively. The objective lens of a Hamamatsu ORCA Flash4.0 sCMOS camera gives an effective pixel size of 2.45 μm. For a region of interest of 1500 x 900 pixels the acquisition time can achieved 10 ms.

The experimental protocol is first to cold compress the cell to the target pressure. Due to compaction of the assembly parts, the strain markers may then appear deformed or tilted on the X-ray image, but without effect on the further strain monitoring (**Figure 2**). Afterward, temperature is raised by steps, and oscillations are applied according to the sine wave profile configuration. The usual settings for torsional loadings are 1 to 5 degrees for the top anvil rotation, over 100 to 1000 s sine wave period, and between 5 to 20 successive cycles. Meanwhile, radiographic images are recorded at high frequencies, producing an image sequence of thousands of frames that traces the motion of the sample/alumina strain markers as a function of time.

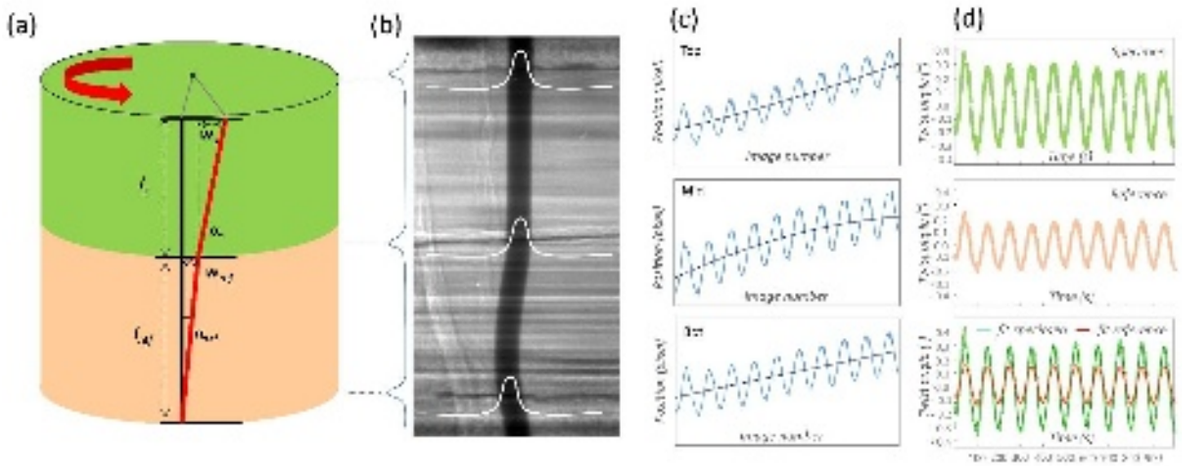

Figure 3 – Principle of the forced-oscillation technique to measure strain energy dissipation. (a) Schematic drawing of the motion of the strain markers during oscillation, and (b) corresponding X-ray radiograph from which the position of the gold foils and tungsten rod are monitored over time. (c) Position of the W rod marker as a function of time (i.e. image number) at the sample and alumina interfaces, and (d) estimated twist angle in degrees for the alumina reference and sample. Represented data are from an olivine specimen and alumina reference at 0.9 GPa and 300 K (see below).

Estimation of anelastic properties

The image sequence is analyzed with an automated ImageJ routine that outputs the sinusoidal curves of the twist angle of the sample (α_s) and reference (α_{ref}) as a function of time, during the cyclic loading. The image processing scheme is depicted in **Figure 3**. It first includes, for each frame, the determination of the horizontal offset of the tungsten rod in the sample (w_s) and reference (w_{ref}) obtained by fitting a Gaussian function along the absorption profile. The round shape and the diameter of 90 μm of the tungsten generate a strong absorption signal on the X-ray images which helps this profile fitting. The offset defines sine waves of few pixels amplitude superimposed to a non-linear baseline that is further subtracted by a second order polynomial fit. This non-linear motion comes from a translation of the whole assembly relative to the X-ray beam as a result of gasket extrusion. The lengths of the sample (l_s) and reference (l_{ref}) as defined by the location of the gold wires markers are also measured. Actually, we did not observed any resolvable change in lengths whatever the rotation angle of the anvils, meaning that the applied torque generates only simple shear. The twist angles of the sample and reference are then calculated according to $\alpha_s = \text{atan}\,(w_s/l_s)$, and $\alpha_{ref} = \text{atan}\,(w_{ref}/l_{ref})$, respectively. These two curves are finally fitted to a sinusoidal equation $\alpha_{s(ref)} = A_{s(ref)} \sin(\omega t + \delta_{s(ref)})$ where A is the amplitude, t is time, and δ is a phase angle. The shear attenuation factor (Q_G^{-1}) is determined from the phase angle lag $\Delta\delta_{s\text{-}ref}$ between the sample and reference according to $Q_G^{-1} = \tan(\Delta\delta)$. The shear modulus is obtained from the A_{ref}/A_s amplitude ratio and the elastic modulus of the reference material.

RESULTS AND DISCUSSION

Calibration of the forced-oscillation apparatus

In order to check the integrity of the present forced oscillation technique, it is necessary to investigate any contamination of the relative amplitudes and phases of the twist angle sinusoids. Potential sources of errors include (i) any mechanical interaction between the specimen/standard set and the boron-epoxy pressure medium, (ii) sliding along the MgO rods, specimen and standard interfaces, or (iii) some image artefacts affecting the location of strain markers. We therefore conducted initial tests at the ESRF synchrotron in which the specimen was replaced by a cylinder of Al_2O_3 of the same composition and dimensions as the one used for the elastic standard. We carried out two sets of measurements under 3.1 GPa pressure, at ambient temperature and 800°C, respectively. For each P-T point, the mechanical testing was performed at conditions of 2 degrees rotation angle - 200 s period, and 1 degree rotation angle – 100 s period.

The twist angle versus time curves are shown in **Figure 4**. The values of the twist angles for the top and bottom Al_2O_3 rods correspond to a $\sim 10^{-3}$ magnitude of strain. These twist angles are consistent with the expected amount for the 2 degrees torsion of a 6.5 mm long assembly (*i.e.* the length of the sample plus reference and MgO rods); meaning that the rotation of the anvils is transmitted to the sample assembly with no loss at the anvil-gasket interface. For some runs, the position of both the top, middle and lower interfaces exhibit some non-sinusoidal spikes (see **Figure 3c**) that translate into similar artefacts on the twist angle curves (**Figure 4**). These features are reproducible over cycles which seems to rule out an origin from sliding on an interface. Instead, they appear to be somehow associated with reversing direction of rotation, being more pronounced whit increasing load, when the rotation angle is larger or when the oscillating period is longer, so that we suspect some slack in the gearbox to be their cause. Being reproducible, these parasitic motions do not significantly affect the sine wave fitting of the twist angle curves, and hence the determination of the Q_G^{-1} and G parameters. In all runs, the top and bottom Al_2O_3 sinusoids are in phase with amplitude ratio close to one, providing compelling evidence that there is no compliance associated with the interfaces, nor any significant effect of the pressure medium and/or graphite furnace. These findings validate the synchrotron imaging method to quantify oscillation strain and the image processing scheme to retrieve the mechanical properties.

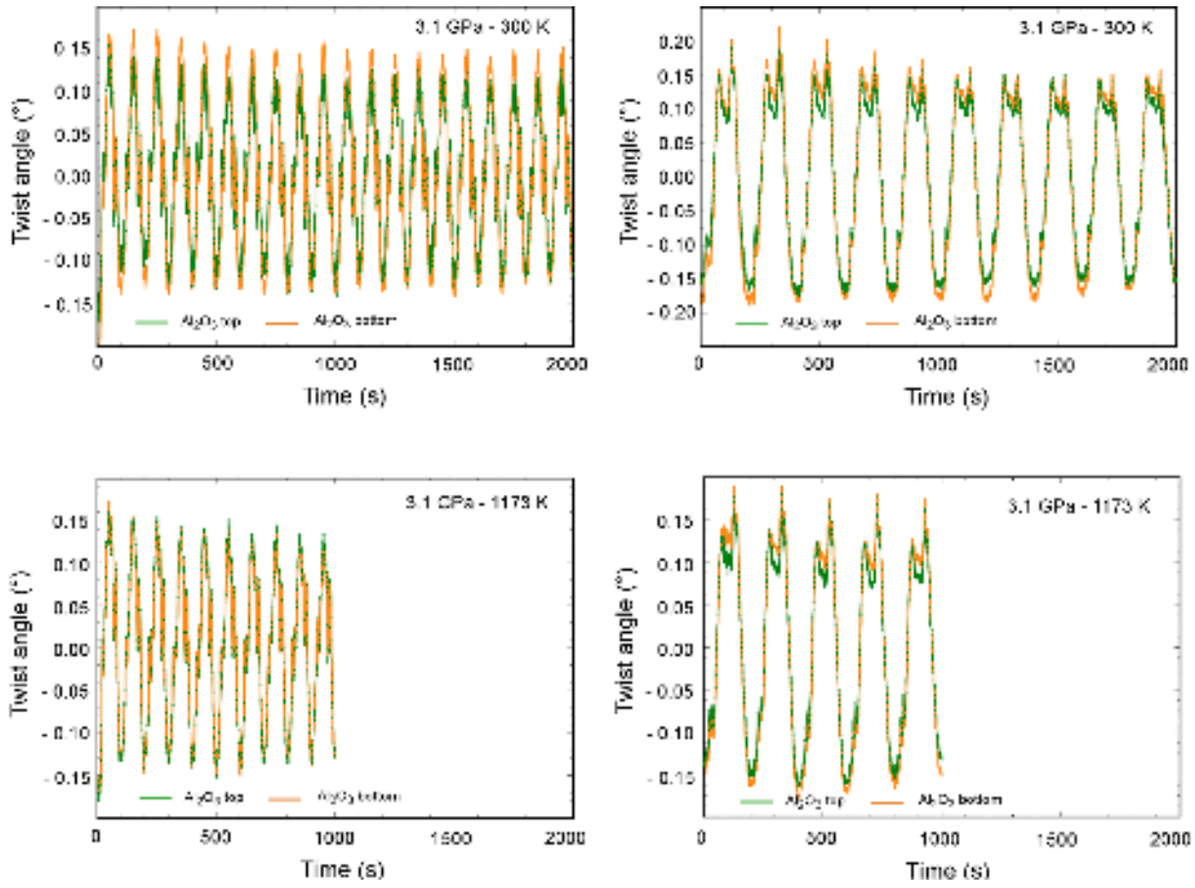

Figure 4 – Twist angle vs. time curves for Al_2O_3-Al_2O_3 test experiments at 3.1 GPa and 300 K-1173 K, and 100 - 200 s oscillation periods, respectively

Preliminary measurements on San Carlos olivine aggregates

To demonstrate the capabilities of the present forced-oscillation technique, we carried out experiments on San Carlos polycrystalline olivine. This phase is one of the most abundant minerals in the mantle, so that the knowledge of its elastic and anelastic properties are critical parameters to understand and model the Earth's interior. Several previous studies have investigated the viscoelastic behavior of olivine both under ambient (Guéguen *et al.*, 1989; Gribb and Copper, 1998) or high pressures (Jackson *et al.*, 2002; Li and Weidner, 2007; Yoshino *et al.*, 2016) to compare with our preliminary measurements. The starting material consisted of natural San Carlos $(Fe_{0.1}Mg_{0.9})_2SiO_4$ crystals, powdered and hot-pressed at 4 GPa – 1000°C for 24 hours to achieve a fine 1-10 μm grain size and a low porosity. Cylindrical samples, respectively 0.48 mm in length and 2.9 mm in diameter were loaded in series with the Al_20_3 (Alfa Aesar^{TM}-Al23) reference. In a first loading, the cell assembly was cold compressed and then heated by steps at 1020 K, 1380 K and 1490 K for the mechanical tests. In a second loading, pressure was first increase to 1.6 GPa at 300 K, with subsequent heating at 1130 K, 1430 K and 1560 K. For all P-T points, the forced-oscillation measurements were performed at

conditions of 2 degrees rotation angle – 200 s period, and X-ray images were recorded at 1 Hz. A SEM image of the recovered sample is shown in **Figure 5**.

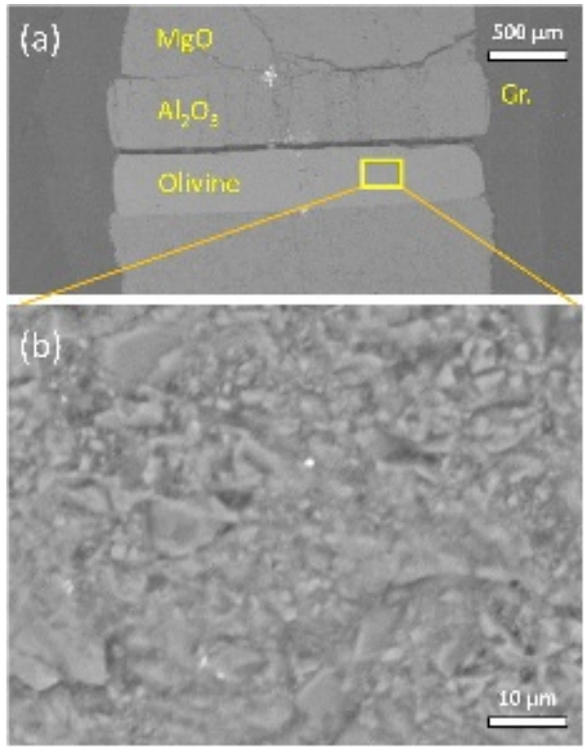

Figure 5 – Electron backscattered images of the sample charge after experiment showing (a) the assembly parts: MgO rod, Al_2O_3 reference, Olivine specimen, Gr. Graphite furnace; and (b) the microstructure of the olivine specimen with 1 – 10 µm grain sizes.

Figure 6 displays the twist angle vs. time curves for each P-T point, and the fits to sinusoids for the olivine and alumina reference. **Figure 7** shows an enlarged view of these curves for the 0.9 GPa – 1380 K data, as well as the corresponding plot for the specimen twist angle against the alumina reference. In such a graph, the deviation from linearity, *i.e.* the appearance of an elliptic shape, is a manifestation of anelasticity, and the surface of this loop represents the amount of energy dissipated (*e.g.* Tisato and Madonna, 2012). The twist angle vs. time curves show the presence of a visible phase lag, and hence attenuation, for temperatures above about 1300 K, along with a marked decrease of the shear modulus. This dispersion of the modulus results from the increase of shear attenuation with temperature.

The attenuation factors (Q_G^{-1}) obtained at 0.9 GPa – 1380 K and 1.6 GPa – 1430 K fall within the range of previous estimates for olivine at ambient and high pressures (**Figure 8**) using either axial or torsional loading techniques (Gribb and Copper, 1998; Tan *et al*., 2001; Jackson *et al*., 2002; Yoshino *et al*., 2016). The temperature dependence of attenuation for the present 0.005 Hz measurements is in broad agreement with literature data obtained at 0.01 Hz on polycrystalline olivine; although a more precise comparison would require to investigate in details the grain size and frequency dependence of the attenuation. We could not determine the

attenuation for temperature beyond 1430 K since the strain curves did not follow anymore the sinusoidal torsion imposed by the anvils. This may point to the onset of plastic strain in the sample or alumina, or any sliding at interfaces. Grain growth is also efficient at high temperature and may affect the attenuation factor for samples where the strain energy dissipation is controlled by grain-boundary sliding processes.

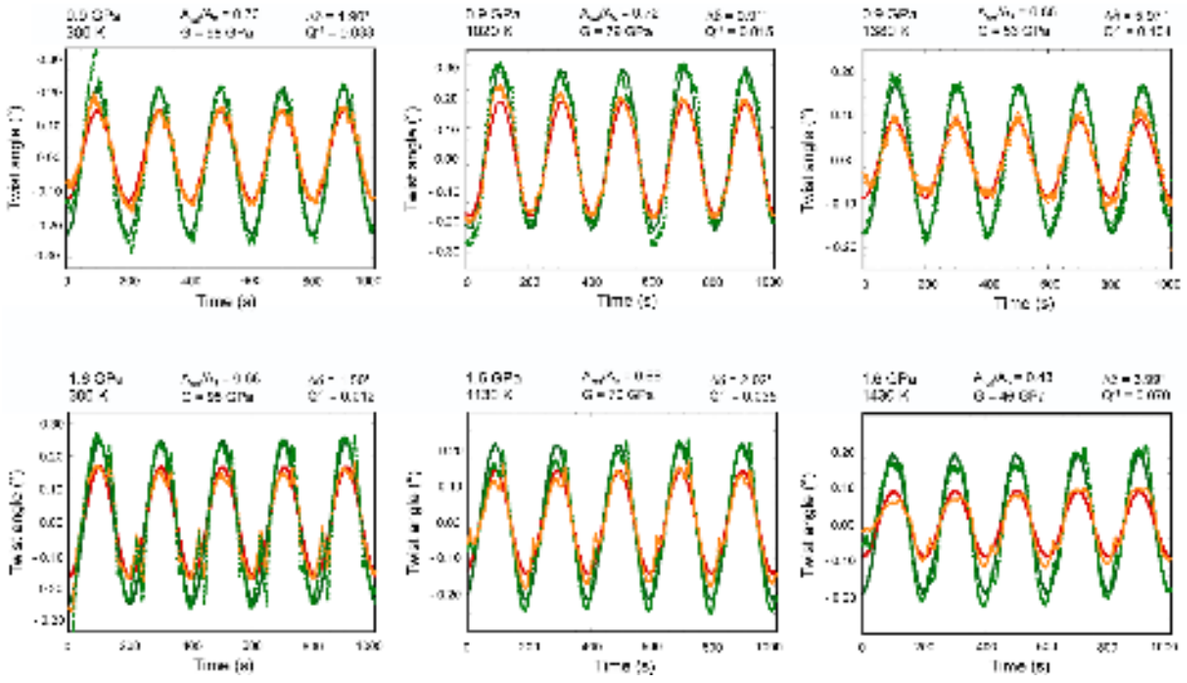

Figure 6 – Twist angle vs. time curves for the San Carlos olivine sample (green dots) and Al_2O_3 reference (orange dots) at specified PT conditions. The forced-oscillation were performed at conditions of 2 degrees rotation angle – 200 s period. Attenuation factors (Q^{-1}) and shear moduli (G) are determined from the phase lag and amplitude ratio estimated from the sinusoid fits to strain curves (dark green and red lines for the olivine sample and alumina reference fits, respectively).

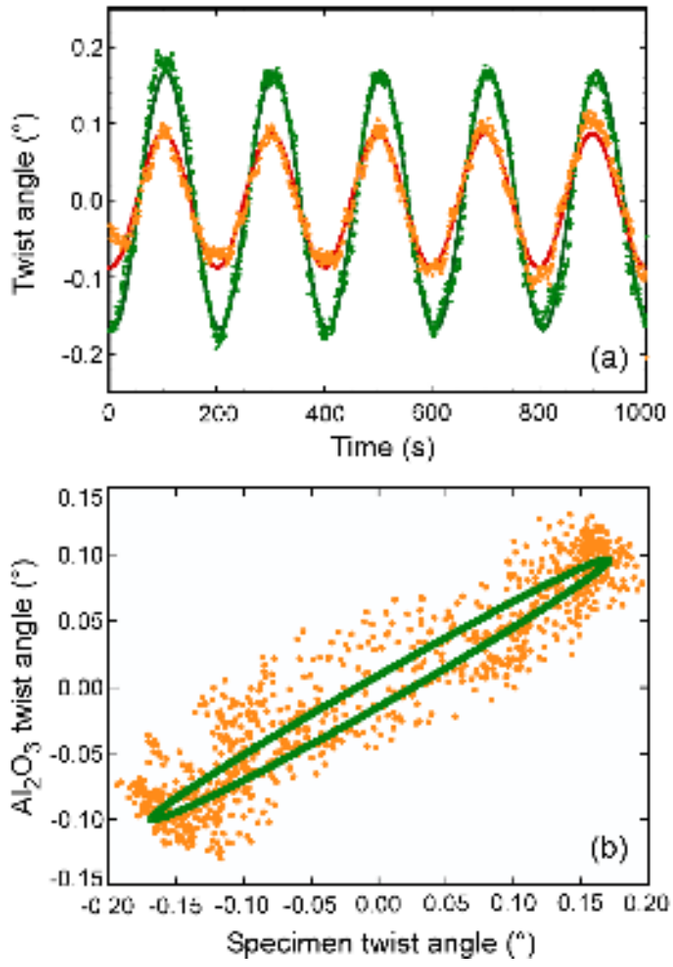

Figure 7 – (a) Detailed view of the twist angle vs. time curve for the olivine-Al_2O_3 reference at conditions of 0.9 GPa – 1380 K and sinusoidal loading with period of 200 s; and (b) the corresponding hysteresis loop. The elliptic shape is a manifestation of anelasticity, and results in a Q^{-1} factor of 0.104.

These preliminary data demonstrate that forced-oscillations in the RoToPEc device combined with synchrotron X-ray imaging is an effective method to study the anelastic properties of materials under extreme conditions, and quantify the effect of temperature, pressure, frequency and grain size on energy dissipation. To date, this method can operates up to 5 GPa within a frequency range from 0.001 to 0.1 Hz. The magnitude of strain achieved is about 10^{-3} while the upper limit of strain to stay in the linear regime domain may be as low as 10^{-4} for some minerals (Guéguen *et al*., 1989). Further developments to achieve 10^{-4} strain will involve the increase of sample length, the reduction of rotation angle and improvement of X-ray radiography resolution. The use of sintered diamond anvils and/or toroidal gaskets (Kono *et al.*, 2015) will also enlarge the X-ray window available for CT imaging in order to expand the technique to higher pressure.

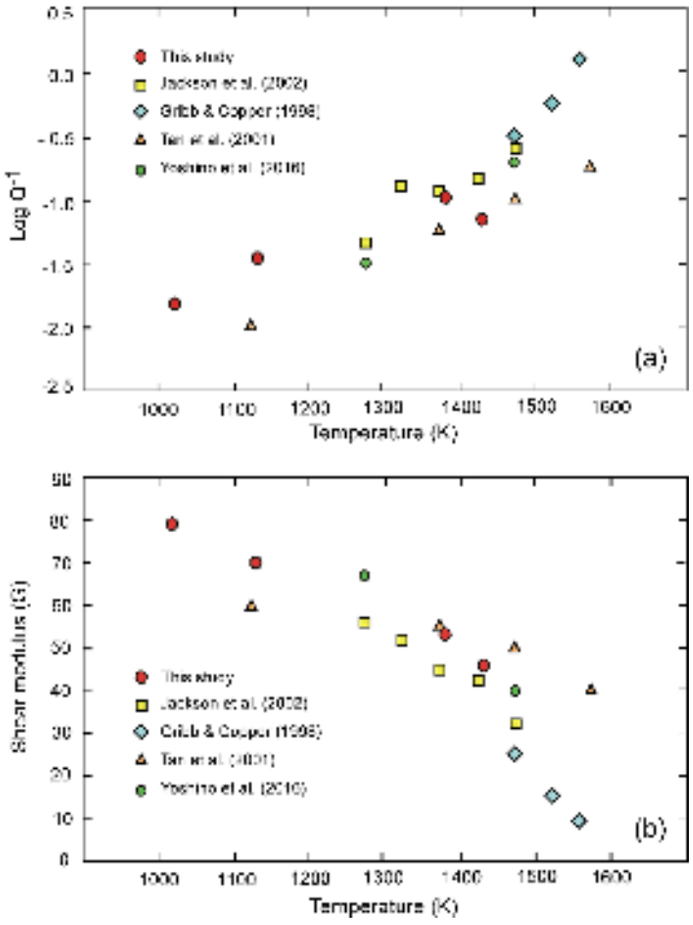

Figure 8 – (a) Attenuation factor (log Q_G^{-1}) vs. temperature and (b) shear modulus (G) vs. temperature for olivine aggregates at frequency of 10 - 5 mHz and pressures between 1 atm to 1.6 GPa, as determined by Gribb & Copper (1998) for 3 μm grain-size Balsam Gap olivine, Tan et al. (2001) for 30 μm grain-size San Carlos olivine, Jackson et al. (2002) for 3-12 μm grain-size Fo90 olivine, Yoshino et al. (2016) for 3 μm grain size San Carlos olivine, and the present study for 1-10 μm grain-size San Carlos olivine

DATA AVAILABILITY

The data that support the findings of this study are available from the corresponding author upon reasonable request.

ACKNOWLEDGMENTS

We acknowledge the European Synchrotron Radiation Facility and Synchrotron SOLEIL for the allocation of beamtimes. We are grateful to S. Bauchau, H. Cardon, J.P. Deslandes, and S. Peuble for technical support during the experiments. This work was financially supported by the French 'Réseau Hautes Pressions', a CNRS-MITI grant 'Instrumentation aux limites', and the CNRS-INSU PNP program.

REFERENCES

Adenis,A., Debayle, E. and Ricard, Y. (2017) Attenuation tomography of the upper mantle, *Geophys. Res. Lett*., 44, 7715–7724, doi:10.1002/2017GL073751.

Aki, K and Richards, P.G. (1980) *Quantitative Seismology, theory and Methods*, W. H. Freeman and Co., 932 pp., San Francisco.

Bagdassarov N.S. and Dingwell, D.B. (1993) Frequency dependent rheology of vesicular rhyolite, *J. Geophys. Res*., 98, B4, 6477-6487.

Berckhemer, H., W. Kampfmann, E. Aulbach, and H. Schmeling (1982). Shear modulus and Q of forsterite and dunite near partial melting from forced oscillation experiments, *Phys. Earth Planet. Inter*., 29, 30– 41.

Besson JM, Nelmes RJ, Hamel G, Loveday JS, Weill G and Hull S. (1992) Neutron powder diffraction above 10-GPa, *Physica B*., 180-181, 907-910.

Cooper, R.F. (2002) Seismic Wave Attenuation: Energy Dissipation in Viscoelastic Crystalline Solids, in *Rev. Mineral. Geochem.*, Mineralogical Society of America, Washington, 253-290.

Gribb, T.T., and Copper, R.F. (1998). Low-frequency shear attenuation in polycrystalline olivine: grain boundary diffusion and the physical significance of the Andrade model for viscoelastic rheology, *J. Geophys. Res*., 103, 22,267-22,279.

Guéguen, Y., Woigard, J. and Darot, M. (1981). Attenuation mechanisms and anelasticity in the upper mantle, in *Anelasticity in the Earth*, pp. 86–94, Stacey, F.D., Paterson, M.S. & Nicholas, A. (Eds), American Geophysical Union, Washington DC.

Gueguen. Y., Darot, M., Mazot, P. and Woirgard, J. (1989) Q-1 of forsterite single crystals, *Phys. Earth Planet. lnter*., 55, 254-258.

Guéguen, Y. and Palciauskas, V. (1994) *Introduction to the physics of rocks*, Princeton University Press, Princeton, 294 pp.

Gung, Y. and Romanowicz,B. (2004) Q tomography of the upper mantle using three component long-period waveforms, *Geophys. J. Int*., 157, 813–830

Jackson, I. (1993) Progress in the experimental study of seismic wave attenuation, *Annu. Rev. Earth Planet. Sci*. 21:375-406.

Jackson, I. (2007) Properties of Rocks and Minerals – Physical Origins of Anelasticity and Attenuation in Rock, in *Treatise on Geophysics*, G. Schubert (Ed), Elsevier, 493-525.

Jackson,I., Fitz Gerald, J.D., Faul, U.H., and Tan, B.H. (2002). Grain-size-sensitive seismic wave attenuation in polycrystalline olivine, *J. Geophys. Res*., 107, doi: 10.1029/ 2001JB001225.

Jackson, I., and Paterson, M.S. (1993). A high-pressure high-temperature apparatus for studies of seismic wave dispersion and attenuation, *Pure App. Geoph*., 141, 445-466.

Karato, S., and Spetzler, H.A. (1990). Defect microdynamics in minerals and solid-state mechanisms of seismic wave attenuation and velocity dispersion in the mantle, *Rev. Geophys*., 28, 399– 421

King A, Guignot N, Zerbino P, Boulard E, Desjardins K et al. (2016) Tomography and imaging at the PSICHE beamline of the SOLEIL synchrotron, *Rev. Sci. Instrum*., 87, 093704, doi.org/10.1063/1.4961365.

Knopoff, L. (1964). Q, *Rev. Geophys*., 2, 625–660, doi: 10.1029/RG002i004p00625.

Li, L. and Weidner, D.J. (2008). Effect of phase transitions on bulk dispersion and attenuation: implications for the earth, *Nature*, 454, 984-986.

Mezouar, M., et al. (2005), Development of a new state-of-the-art beamline optimized for monochromatic single-crystal and powder X-ray diffraction under extreme conditions at the ESRF, *J. Synchrotron Rad.*, 12, 659–664.

Ota, K. and Pezzotti, G. (1996) Anelastic and plastic relaxation in polycrystalline alumina and single-crystal sapphire, *J. Mater. Res*., 11, 2785–2789.

Philippe, J., Le Godec, Y., Mezouar, M., Berg, M., Bromiley, G., Bergame, F., Perrillat, J.P., Alvarez-Murga, M., Morand, M., Atwood, R., King, A. & Régnier, S. (2016). *High Pressure Res*., doi: 10.1080/08957959.2016.1221951

Pozgay, S., Wiens,D., Conder, J., Shiobara, H. and Sugioka, H. (2009). Seismic attenuation tomography of the Mariana subduction system: implications for thermal structure, volatile distribution, and slow spreading dynamics, *Geochem. Geophys. Geosyst*., 10, Q04X05, doi:10.1029/2008GC002313.

Speziale, S., Zha, C.S., Duffy, T.S., Hemley, R.J. and Mao, H.K. (2001) Quasi-hydrostatic compression of magnesium oxide to 52 GPa: Implications for the pressure-volume-temperature equation of state, *J. Geophys. Res. Lett*., 106, 515-528.

Stachnik, J. C., Abers, G.A. and Christensen, D.H. (2004). Seismic attenuation and mantle wedge temperatures in the Alaska subduction zone, *J. Geophys. Res*., 109, B10304, doi:10.1029/2004JB003018

Tan, B.H., Jackson, I., Fitz Gerald, J.D. (2001) High temperature viscoelasticity of fine-grained polycrystalline olivine, *Phys. Chem. Min*., 28, 641-664.

Tisato, N., Madonna, C. (2012) Attenuation at low seismic frequencies in partially saturated rocks: Measurements and description of a new apparatus, J. App. Geophys., 86, 44-53.

Webb, S., Jackson, I., and Fitz Gerald, J.D. (1999). Viscoelasticity of the titanate perovskites CaTiO3 and SrTiO3 at high temperature, *Phys. Earth Planet. Int*., 115, 259-291.

Webb, S., and Jackson, I. (2003) Anelasticity and microcreep in polycrystalline MgO at high temperature: an exploratory study, *Phys. Chem. Mineral*., 30, 157-166.

Yoshino, T., Yamazaki, D., Tange, Y. and Higo, Y. (2016). Short-period cyclic loading system for in situ Xray observation of anelastic properties at high pressure, *Rev. Sci. Inst*., 87, 105106, doi: 10.1063/1.4963747

FIGURES CAPTIONS

Figure 1 – 3D view of the 450 ton V7 Paris-Edinburgh press with the RoToPEc module, and picture of its installation on beamline ID27 of the ESRF.

Figure 2 – (left) Cell assembly used for the forced-oscillation measurements, and (right) representative X-ray radiograph through the sample and alumina standard. Highly absorbing features are the gold and tungsten strain markers.

Figure 3 – Principle of the forced-oscillation technique to measure strain energy dissipation. (a) Schematic drawing of the motion of the strain markers during oscillation, and (b) corresponding X-ray radiograph from which the position of the gold foils and tungsten rod are monitored over time. (c) Position of the W rod marker as a function of time (i.e. image number) at the sample and alumina interfaces, and (d) estimated twist angle in degrees for the alumina reference and sample. Represented data are from an olivine specimen and alumina reference at 0.9 GPa and 300 K (see below).

Figure 4 – Twist angle vs. time curves for Al_2O_3-Al_2O_3 test experiments at 3.1 GPa and 300 K-1173 K, and 100 - 200 s oscillation periods, respectively.

Figure 5 – Electron backscattered images of the sample charge after experiment showing (a) the assembly parts: MgO rod, Al_2O_3 reference, Olivine specimen, Gr. Graphite furnace; and (b) the microstructure of the olivine specimen with 1 – 10 μm grain sizes.

Figure 6 – Twist angle vs. time curves for the San Carlos olivine sample (green dots) and Al_2O_3 reference (orange dots) at specified PT conditions. The forced-oscillation were performed at conditions of 2 degrees rotation angle – 200 s period. Attenuation factors (Q^{-1}) and shear moduli (G) are determined from the phase lag and amplitude ratio estimated from the sinusoid fits to strain curves (dark green and red lines for the olivine sample and alumina reference fits, respectively).

Figure 7 – (a) Detailed view of the twist angle vs. time curve for the olivine-Al_2O_3 reference at conditions of 0.9 GPa – 1380 K and sinusoidal loading with period of 200 s; and (b) the corresponding hysteresis loop. The elliptic shape is a manifestation of anelasticity, and results in a Q^{-1} factor of 0.104.

Figure 8 – (a) Attenuation factor (log Q_G^{-1}) vs. temperature and (b) shear modulus (G) vs. temperature for olivine aggregates at frequency of 10 - 5 mHz and pressures between 1 atm to 1.6 GPa, as determined by Gribb & Copper (1998) for 3 μm grain-size Balsam Gap olivine, Tan et al. (2001) for 30 μm grain-size San Carlos olivine, Jackson et al. (2002) for 3-12 μm grain-size Fo90 olivine, Yoshino et al. (2016) for 3 μm grain size San Carlos olivine, and the present study for 1-10 μm grain-size San Carlos olivine.

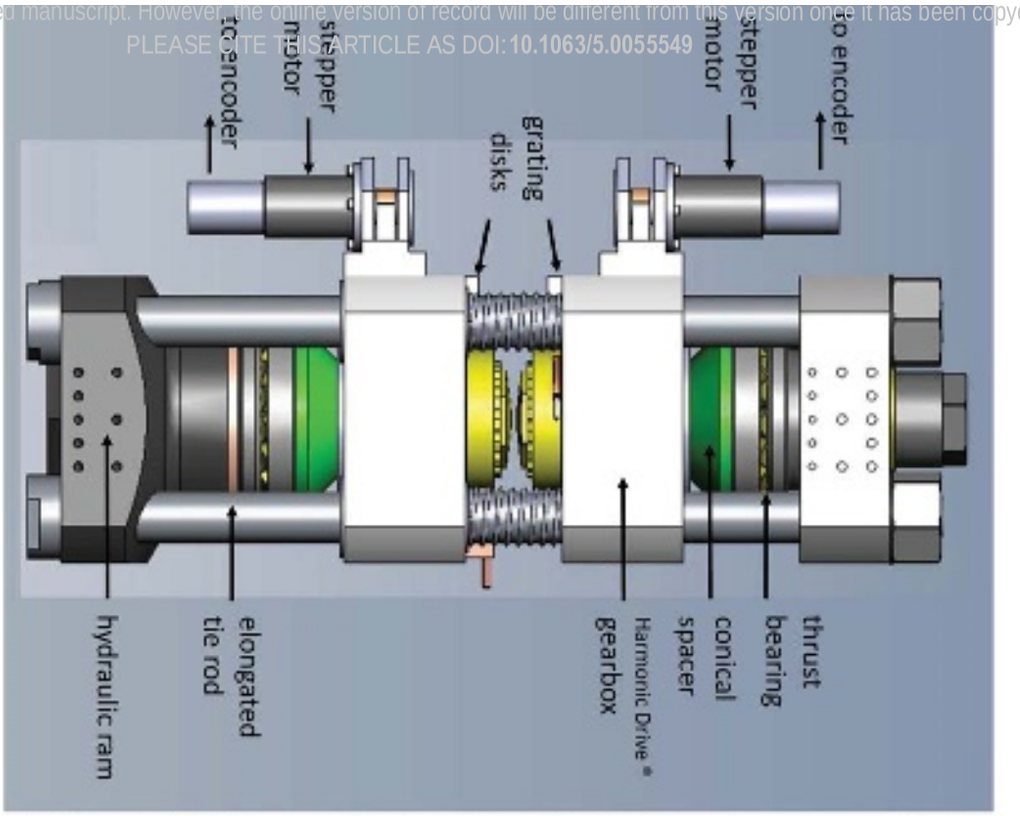

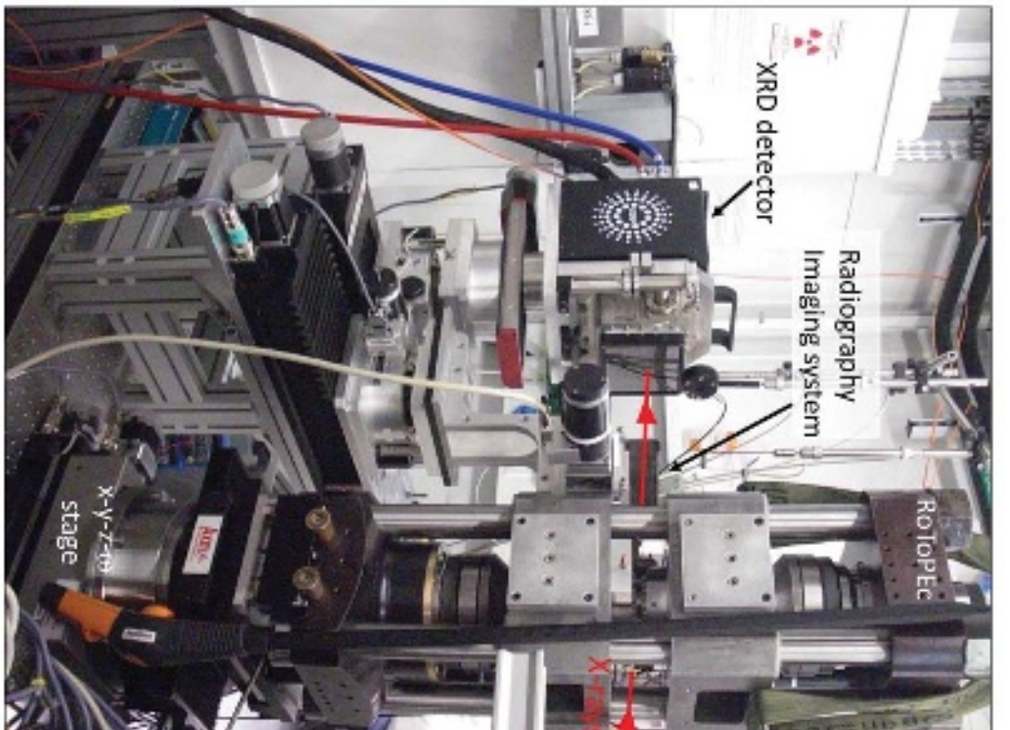

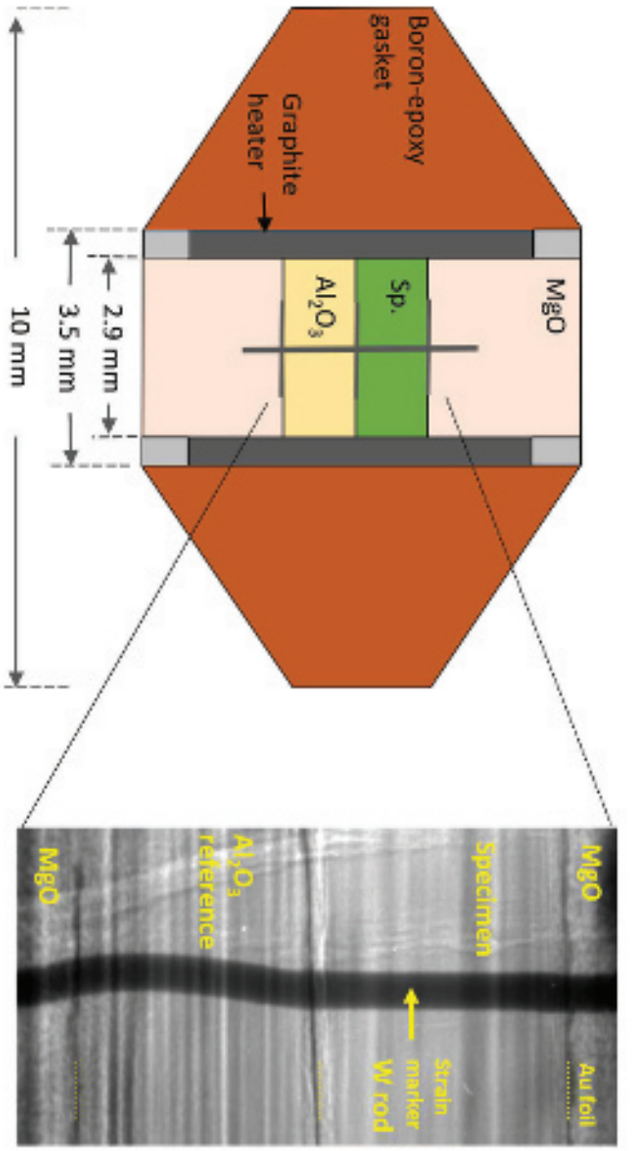

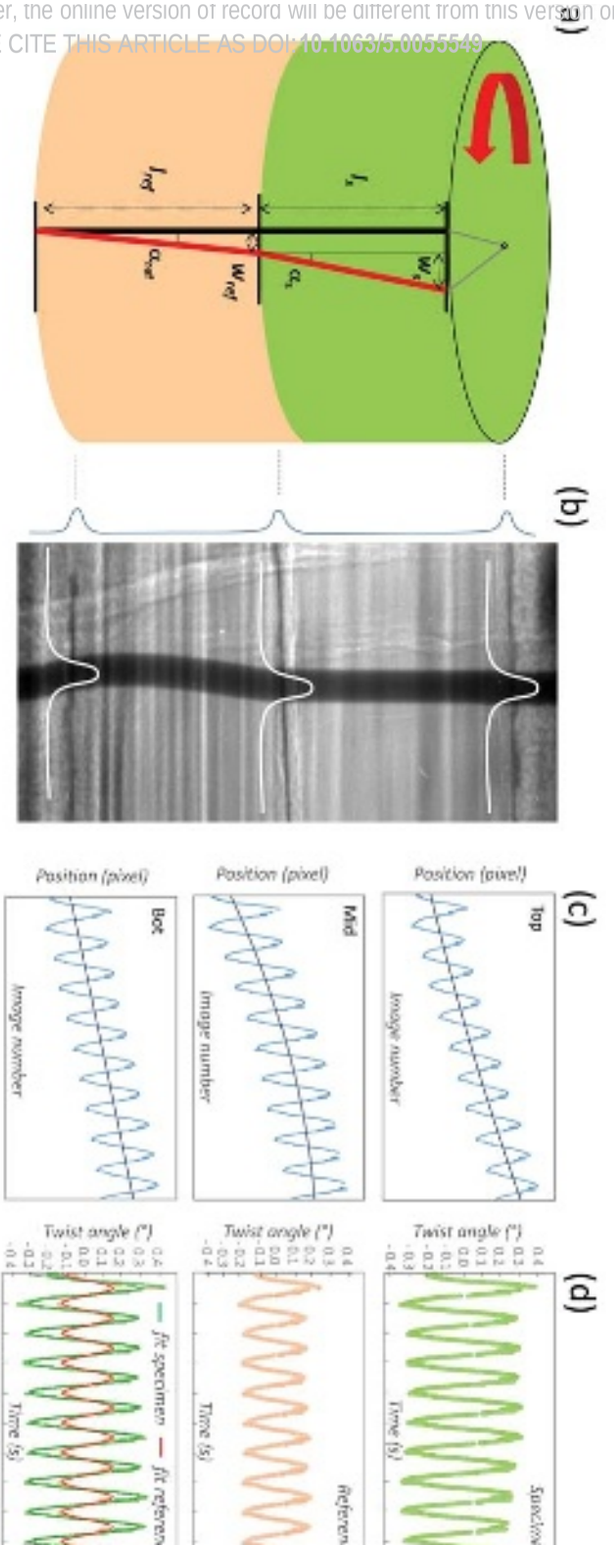

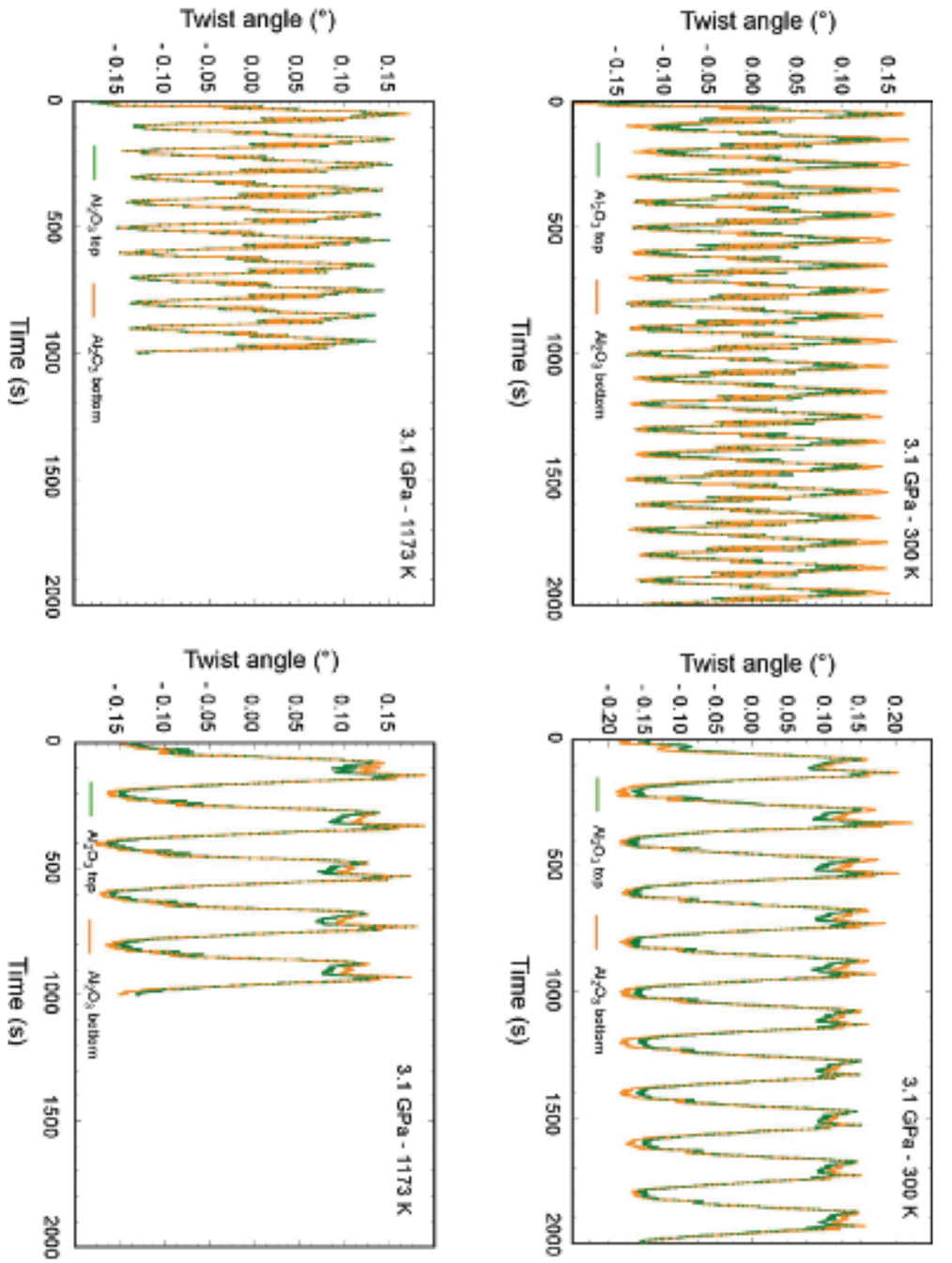

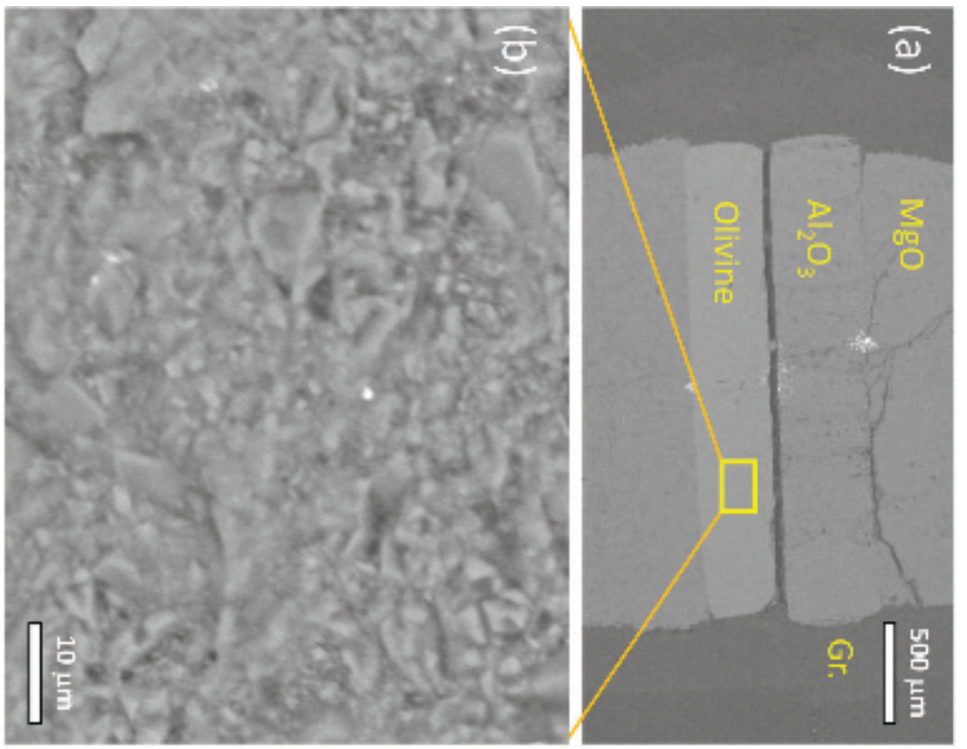

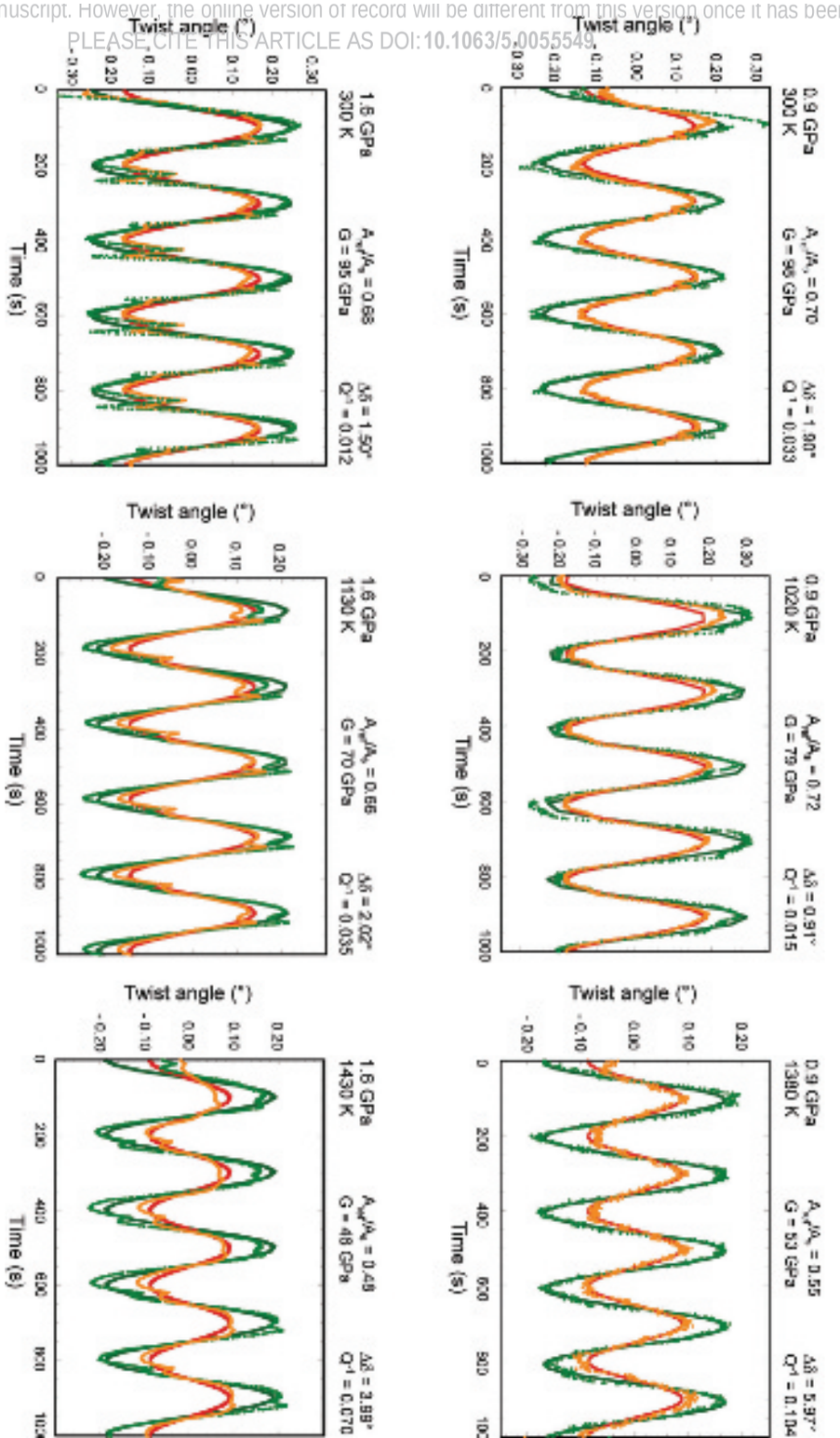

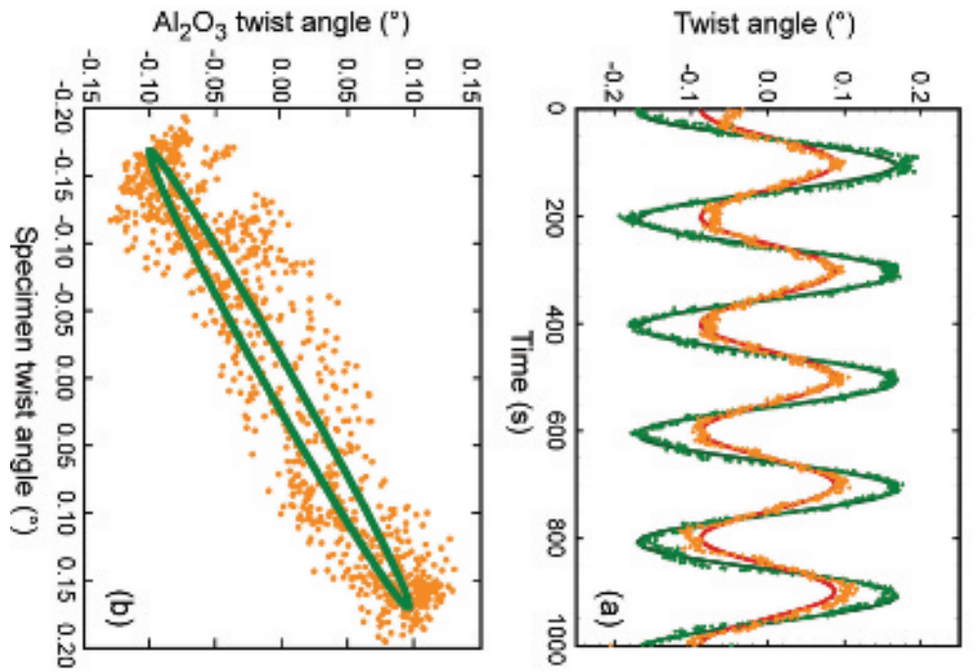

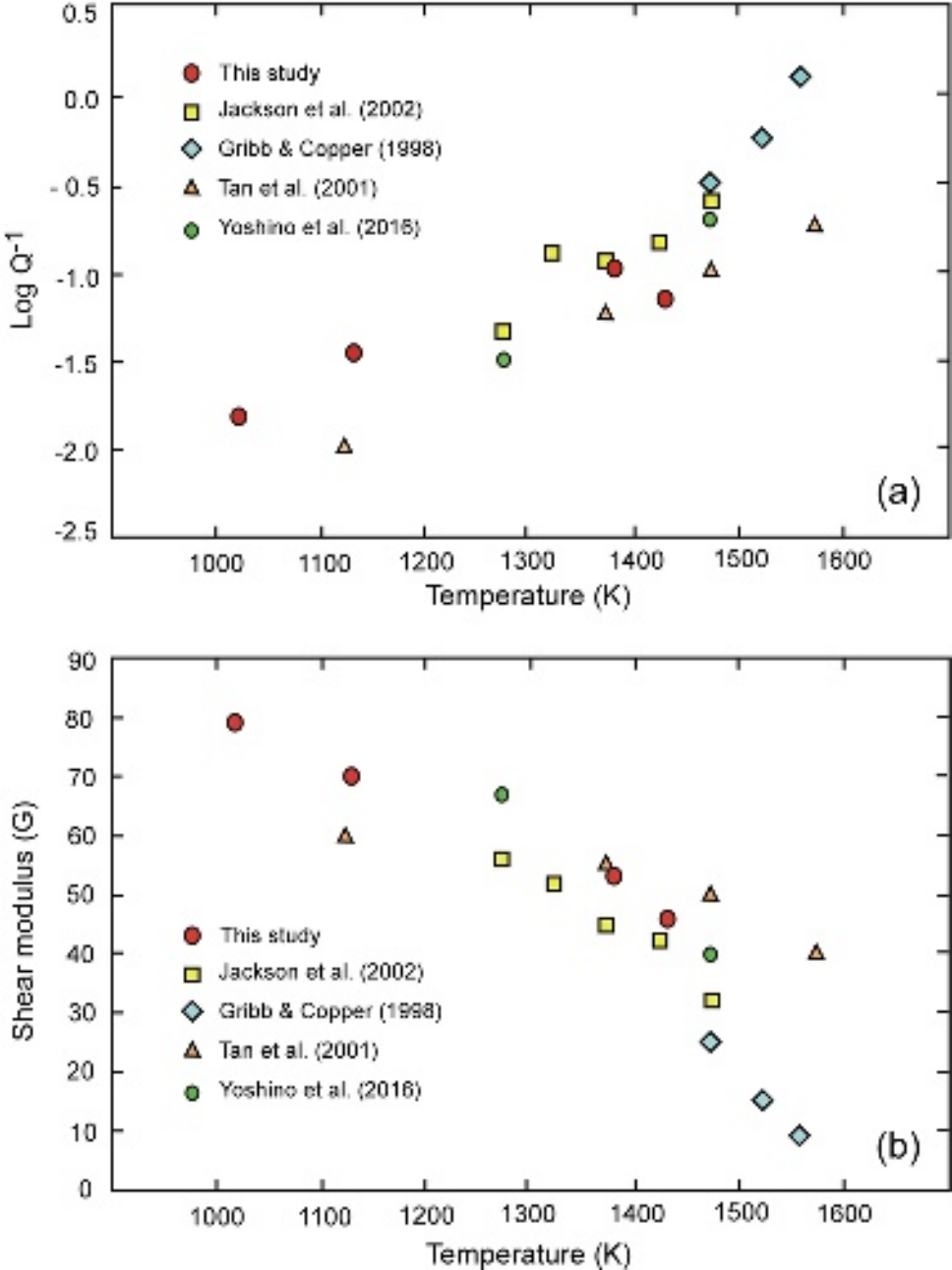
This study
Jackson et al. (2002)
Gribb & Copper (1998)
Tan et al. (2001)
Yoshino et al. (2016)
Log Q-1
Temperature (K)
(a)
Shear modulus (G)
Temperature (K)
(b)